Entanglement-preserving measurement of the Bell parameter on a single entangled pair

Entanglement-preserving measurement of the Bell parameter on a single entangled pair

IOP Publishing Quantum Sci. Technol. 9 (2024) 045027 https://doi.org/10.1088/2058-9565/ad6a37

Quantum Science and Technology

OPEN ACCESS

RECEIVED
20 February 2024

REVISED
26 July 2024

ACCEPTED FOR PUBLICATION
1 August 2024

PUBLISHED
20 August 2024

PAPER

Entanglement-preserving measurement of the Bell parameter on a single entangled pair

Salvatore Virzì[1], Enrico Rebufello[1], Francesco Atzori[1,2], Alessio Avella[1], Fabrizio Piacentini[1,*], Rudi Lussana[3], Iris Cusini[3], Francesca Madonini[3], Federica Villa[3], Marco Gramegna[1], Eliahu Cohen[4], Ivo Pietro Degiovanni[1,5] and Marco Genovese[1,5]

[1] INRIM, Strada delle Cacce 91, I-10135 Torino, Italy
[2] Politecnico di Torino, Corso Duca degli Abruzzi 24, I-10129 Torino, Italy
[3] Dipartimento di Elettronica, Informazione e Bioingegneria, Politecnico di Milano, Piazza Leonardo da Vinci 32, 20133 Milano, Italy
[4] Faculty of Engineering and the Institute of Nanotechnology and Advanced Materials, Bar Ilan University, Ramat Gan, Israel
[5] INFN, sezione di Torino via P. Giuria 1, 10125 Torino, Italy
[*] Author to whom any correspondence should be addressed.

E-mail: f.piacentini@inrim.it

Keywords: quantum foundations, quantum information, quantum resources, quantum technologies

Abstract

Bell inequalities represent one of the cornerstones of quantum foundations, and a fundamental tool for quantum technologies. Although a lot of effort was put in exploring and generalizing them, because of the wave function collapse it was deemed impossible to estimate the entire Bell parameter from one entangled pair, since this would involve measuring incompatible observables on the same quantum state. Conversely, here it is reported the first implementation of a new generation of Bell inequality tests, able to extract a Bell parameter value from each entangled pair and, at the same time, preserve the pair entanglement instead of destroying it. This is obtained by exploiting sequences of weak measurements, allowing incompatible observable measurements on a quantum state without collapsing its wave function. On the fundamental side, by removing the need to choose between different measurement bases our approach stretches the concept of counterfactual definiteness, since it allows measuring the entangled pair in all the bases needed for the Bell inequality test, intrinsically eliminating the issues connected with the otherwise not-chosen bases. On the practical side, after our Bell parameter measurement the entanglement within the pair remains (basically) unaltered, hence exploitable for other quantum-technology-related or foundational purposes.

1. Introduction

Since their formulation [1], Bell inequalities [2–4] have been one of the pillars of quantum foundations investigation, and lately became a fundamental tool for quantum technologies [5], e.g. quantum communication [6]. Recently, the scientific community worldwide has put a lot of effort towards exploring them [2, 3, 7–9]; nonetheless, it was deemed impossible to extract information on the full inequality from each entangled pair, since the wave function collapse forbids performing, on the same quantum state, all the measurements needed for evaluating the entire Bell parameter. Another consequence of the wave function collapse is the fact that entanglement is destroyed after the measurement, making it impossible its exploitation for further foundational or technological purposes.

Conversely, here we present the first single-pair Bell inequality test, able to estimate a Bell parameter value from each entangled pair without compromising the entanglement within it. This is achieved by exploiting weak quantum measurements [10–13] in sequence, allowing to measure non-commuting observables on the same quantum state without collapsing it. Such an approach provides new insights into understanding the foundations of quantum mechanics, like the concept of counterfactual-definiteness [14]. Furthermore, it grants unprecedented measurement and technological capabilities: indeed, since the

entanglement remains almost unaltered after the Bell parameter measurement allowing to certify it, one can use it for other practical purposes like, e.g. quantum technology protocols [5].

The huge relevance of Bell inequalities stems from the fact that they allow to discard a whole class of 'classical' theories. In these theories, called local hidden variable theories (LHVTs) [2], all measurement outcomes satisfy the *locality* principle [3, 4, 15] and are pre-determined by some inaccessible 'hidden variables', i.e. they are characterized by an *epistemic* probabilistic trait entirely due to our lack of knowledge on these hidden variables (whose knowledge would allow recovering the determinism of classical physics), in sharp contrast with the *non-locality* and *non-epistemic probability* pertaining to quantum mechanics. A long journey, awarded by the 2022 Nobel prize, has been undergone [2, 3] since their introduction, but eventually loophole-free violations of Bell inequalities were achieved [7–9]. Along the way, one can recall the very first tests [16–18] and the first experiment with space-like separated measurements [19]. However, throughout this whole journey it has always been deemed impossible to extract information on the entire Bell inequality from every entangled pair measured, since the uncertainty principle and the wave function collapse, following rank-1 projective measurements, do not allow performing on the same quantum state all the measurements needed for inferring the entire Bell parameter at once (for this reason, alternative Bell tests relying on compatible observables measurements have been proposed, see e.g. [20]). This means that the 'experimenters' performing the test, conventionally named Alice and Bob, must (randomly) choose, pair by pair, the measurement basis for each of the two entangled particles, that are then combined to extract the Bell parameter. In order to avoid opening loopholes in the test, these choices need to be independent ('freedom-of-choice' loophole) and no communication should be allowed between these measurements ('locality' loophole) [4]. Another consequence of the wave function collapse is that entanglement is destroyed after the measurement, forbidding its exploitation for further foundational or technological purposes.

Here we illustrate an actual paradigm shift in this perspective, since we experimentally demonstrate the possibility of extracting information on the full Bell parameter from each entangled pair measured and, at the same time, still conserving most of the pair entanglement after the measurement, leaving it available for further use (see, e.g. [21]). This is made possible by implementing two weak measurements (WMs) [10–13, 22] in a sequence [23–28] on each particle forming the entangled pair, not only providing new insights into understanding quantum foundations (like the concept of counterfactual-definiteness [14]), but also granting unprecedented measurement/technological capabilities, since our WM approach allows leaving the entanglement almost unaltered after its certification. We note that, in the original spirit of the paper introducing them [10], our measurements being weak means that the coupling between the measured system and the measuring pointer is much smaller than the latter's spread, but we do not employ any postselection stage. Therefore, we do not obtain the so-called 'weak values' characterizing pre- and postselected quantum systems.

WMs have already represented a significant tool for studies on quantum foundations [12], with relevant breakthroughs in quantum technologies [29–31]. In connection with entanglement, they found application in quantum contextuality [32–34], nonlocality [35, 36] and Leggett–Garg inequalities [37–42]. In particular, some experiments started exploring the possibility of testing Bell inequalities and the Einstein–Podolsky–Rosen paradox, considering multiple WMs on a single arm only [43], one WM plus one strong (projective) measurement in both arms [44], or by measuring a hybrid Bell–Leggett–Garg inequality [45]. Conversely, the aforementioned paradigm shift in our experiment relies on the fact that we evaluate the *entire* Bell parameter from each entangled pair detected (although with large uncertainty, typical of WMs): thanks to the weak interaction exploited, only a tiny decoherence is induced on the entangled state (instead of the full decoherence due to the measurement-induced collapse of its wave function) throughout the Bell parameter measurement, allowing to make use of the quantum correlations within the weakly-measured entangled pair for other experiments or quantum technology protocols [5]. An attempt to extract the Bell parameter without separate quantification of the single correlators has also been made [46], but the sharp measurements involved did not allow conserving the state after the measurement, destroying the entanglement. Since our experiment does not require any ability of speaking meaningfully of the definiteness of measurements that have not been performed, we avoid any use of counterfactual definiteness [14] hypothesis, ultimately concluding the debate whether counterfactual definiteness can be an additional hypothesis in Bell inequality tests [47] and cast challenges to some interpretations of quantum mechanics (e.g. the modal ones [48, 49]).

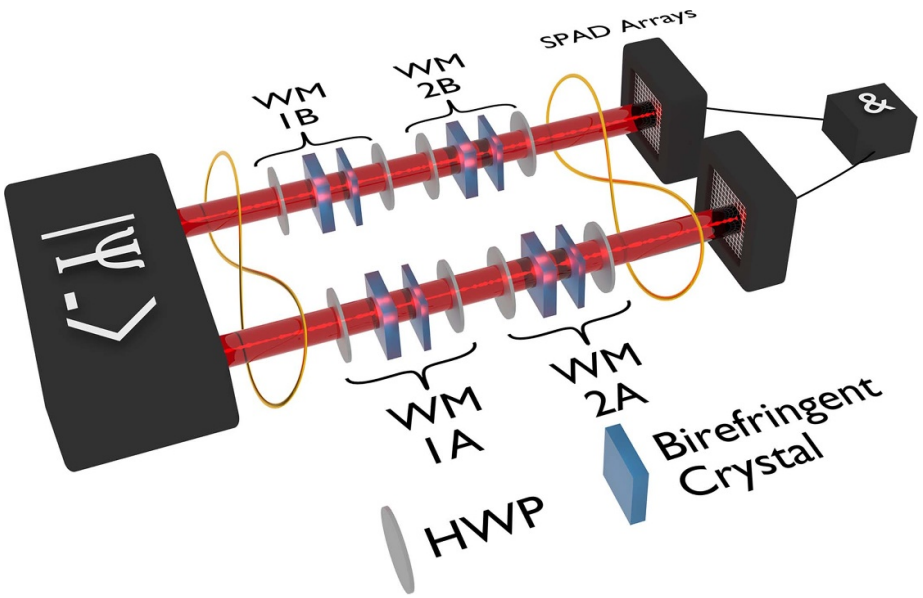

Figure 1. Pictorial scheme of the experiment. An entangled photon source generates polarization-entangled photon pairs in the state $|\psi_-\rangle = (|H_A V_B\rangle - |V_A H_B\rangle)/\sqrt{2}$, addressing them to the Alice (A) and Bob (B) branches. There, each photon undergoes two weak measurements (WMs) in sequence, each realized by a pair of birefringent crystals preceded by a half-wave plate (HWP). The HWPs are responsible for setting the parameters $\alpha_1, \alpha_2, \beta_1, \beta_2$. These measurements induce just a small decoherence on the $|\psi_-\rangle$ state instead of causing the wave function collapse, thus avoiding the total breakdown of the entanglement (represented by the infinity symbol) within the state. Finally, the entangled photons are detected by two spatially-resolving detectors with a time-tagging module (&). A detailed description of the experimental setup is reported in appendix A.

2. Experimental results and discussion

Our aim is to measure a violation of the Clauser–Horne–Shimony–Holt (CHSH) inequality [2]:

$$|\mathcal{S}| = |C(\alpha_1,\beta_1) - C(\alpha_1,\beta_2) + C(\alpha_2,\beta_1) + C(\alpha_2,\beta_2)| \leqslant 2\,, \tag{1}$$

where $C(\alpha_j,\beta_k) = \langle \hat{\sigma}_z(\alpha_j) \otimes \hat{\sigma}_z(\beta_k)\rangle$, $j,k = 1,2$, and $\hat{\sigma}_z(\theta) = U(\theta)\sigma_z U^\dagger(\theta)$, being $U(\theta) = \left(\begin{smallmatrix} \cos\theta & \sin\theta \\ \sin\theta & -\cos\theta \end{smallmatrix}\right)$ and σ_z the third Pauli matrix. We do this by generating polarization-entangled photon pairs in the singlet state $|\psi_-\rangle = (|H_A V_B\rangle - |V_A H_B\rangle)/\sqrt{2}$, being H (V) the horizontal (vertical) polarization component, and sending them to Alice (A) and Bob (B), who measure them twice in a row by means of weak-interaction-based measurements realized by thin birefringent crystals, as illustrated in figure 1 (see appendix A for a detailed description of the experimental apparatus). Each WM couples (weakly) the photon polarization observable with an ancillary spatial degree of freedom orthogonal to the photons propagation direction z (specifically: x_A, y_A for Alice's measurements, x_B, y_B for Bob's). This means that, in our scheme, the ancillas are not separate particles (with respect to the measured ones), but rather separate degrees of freedom pertaining to the same photons undergoing the WM process. By exploiting detectors with two-dimensional spatial resolution, Alice and Bob can extract the information on their polarization measurements, as well as on their cross-correlations, from the X_A, Y_A, X_B, Y_B coordinates set generated by the detection of each entangled photon pair. Our setup allows realizing, for the first time, both joint [50] and sequential [25, 26] WMs on a bipartite state, a task utterly forbidden by traditional (projective) measurement schemes. Specifically, in our experiment both Alice and Bob perform a sequence of two WMs of their photon polarization on the bases respectively defined by the α_1, α_2 and β_1, β_2 parameters, avoiding to collapse the state and, as a consequence, extracting information on the entire Bell parameter $\mathcal{S}$ from each entangled pair.

The results obtained for $\alpha_1 = 0, \alpha_2 = \frac{\pi}{4}, \beta_1 = \frac{\pi}{8}, \beta_2 = \frac{3\pi}{8}$, allowing for a maximal violation of the CHSH inequality, are shown in figure 2. Although the very nature of WMs leads to a large uncertainty on a single measurement event (with the exception of *robust* WMs [51], that anyway cannot be implemented in this kind of scenario), when averaging on several events a significant violation (almost 6 standard deviations) of the classical bound pertaining to LHVTs [2] is achieved: $\mathcal{S}^{\text{ave}} = -(2.79 \pm 0.14)$, in perfect agreement with the Tsirelson bound.

As visible from figure 2, for single measurement events even values of $\mathcal{S}$ much beyond the Tsirelson bound can be obtained, but this should not be regarded as an issue, since the uncertainty associated with

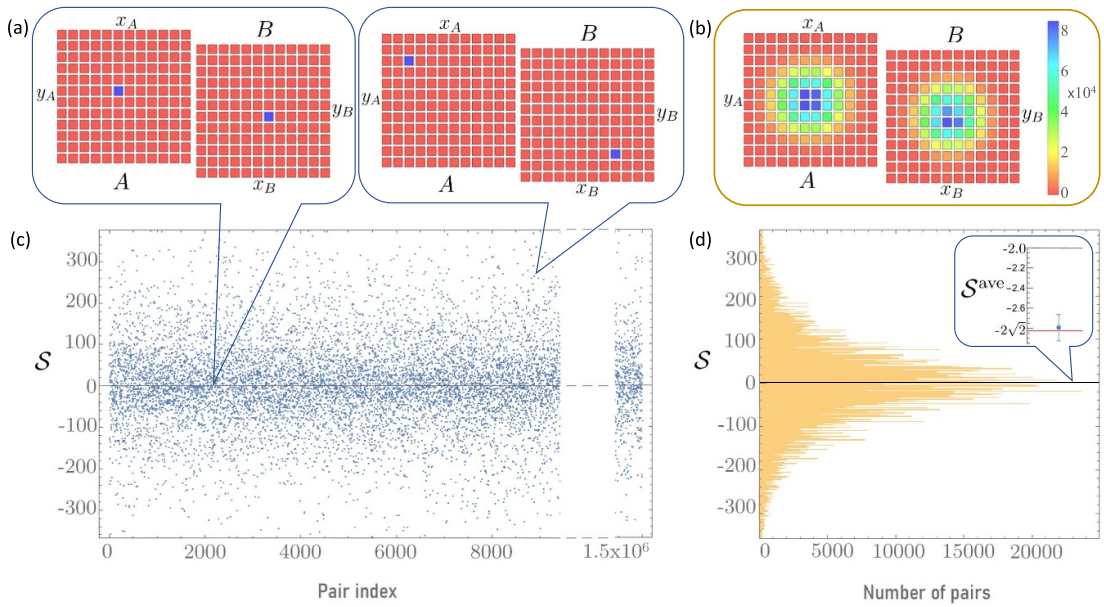

Figure 2. Single-pair estimation of the Bell parameter $\mathcal{S}$. Plot (a): typical entangled photon pair detection events. The blue squares indicate the pixels firing in the spatially-resolving detectors at the end of branch A and B, respectively. The x_A, y_A, x_B, y_B axes indicate the spatial degrees of freedom in which the information of the four polarization weak measurements shown in figure 1 is encoded (see equation (A1) in appendix A). Plot (b): spatial distribution of the two photons exiting the Bell parameter measurement, formed by the integral of all photon pair detection events. Plot (c): estimation of the $\mathcal{S}$ parameter for each photon pair detected. The large variance of the results distribution is the signature of the measurements weakness in the experiment. Plot (d): histogram representing the integral of all the estimated $\mathcal{S}$ values. The blue dot in the inset indicates the average on all the collected events (dark counts subtracted), $\mathcal{S}^{ave} = -(2.79 \pm 0.14)$, in perfect agreement with quantum mechanics Tsirelson bound ($\mathcal{S}^{QM} = -2\sqrt{2}$, red line) and highlighting a 5.6 standard deviations violation of the LHVT bound ($\mathcal{S}^{LHVT} = -2$, black line). The uncertainty associated with the $\mathcal{S}^{ave}$ value (blue vertical line) includes both statistical and systematic contributions (see appendix B for details).

them makes them always compatible with the $|\mathcal{S}| \leqslant 2\sqrt{2}$ interval of 'allowed' values. This situation does not differ from any experiment where a physical quantity is evaluated with a large uncertainty, with the central value of the single measurement outcome eventually resulting out of the physical bounds, but still compatible with them when the associated uncertainty is considered. The aforementioned large variance of the results in our experiment stems from the fact that the spread of the pointer variable (i.e. the width of the Gaussian spatial wave function of the photons generated by our source) is much larger than the spatial shifts induced by our WMs, as required by the definition of WM.

To study the effect of this WM scheme on each entangled pair tested and estimate the entanglement still available at the end of the protocol, we perform the tomographic reconstruction [52] of the quantum state both before (figure 3, plots (a) and (b)) and after (figure 3, plots (c) and (d)) the WM sequence. In both cases, we report as inset the quantum Fidelity $F(\rho^{rec}, \rho_{\psi_-}) = (\mathrm{Tr}(\sqrt{\sqrt{\rho^{rec}}\rho_{\psi_-}\sqrt{\rho^{rec}}}))^2$ [53] between the reconstructed density matrix ρ^{rec} and the singlet state one $\rho_{\psi_-} = |\psi_-\rangle\langle\psi_-|$, as well as the reconstructed state Purity $P = \mathrm{Tr}\left[(\rho^{rec})^2\right]$. The values displayed in figure 3(b) testify the high quality of the singlet state produced by our entangled photon source. The ones shown in figure 3(d) allow appreciating, instead, how the state outgoing the single-pair Bell parameter measurement is still close to the one entering it, a clear sign of the tiny decoherence induced by the four weak measurements and, as a consequence, of the close-to-maximal entanglement still present within the state after the measurement process. Trivially, by making the measurements even weaker we would further decrease the amount of decoherence on the entangled state, at the cost of an increased uncertainty in determining the Bell parameter (or, equivalently, at the cost of increasing the number of required pairs to achieve a certain uncertainty level). Eventually, taking the coupling strength close to zero will amount to almost zero disturbance and infinite number of pairs to be tested.

In order to quantitatively estimate the entanglement present in the two-photon state before and after the Bell parameter measurement, we evaluate the Negativity and Concurrence [54] of the entangled state entering ($\mathcal{N}^{in}$ and $\mathcal{C}^{in}$, respectively) and outgoing it ($\mathcal{N}^{out}$ and $\mathcal{C}^{out}$, respectively). To do this, we follow two different methods: (1) we evaluate them directly from the reconstructed density matrices, obtaining $\mathcal{N}^{in} = 0.981$ and $\mathcal{C}^{in} = 0.979$ for the initial state, and $\mathcal{N}^{out} = 0.937$ and $\mathcal{C}^{out} = 0.894$ for the final one; (2) we

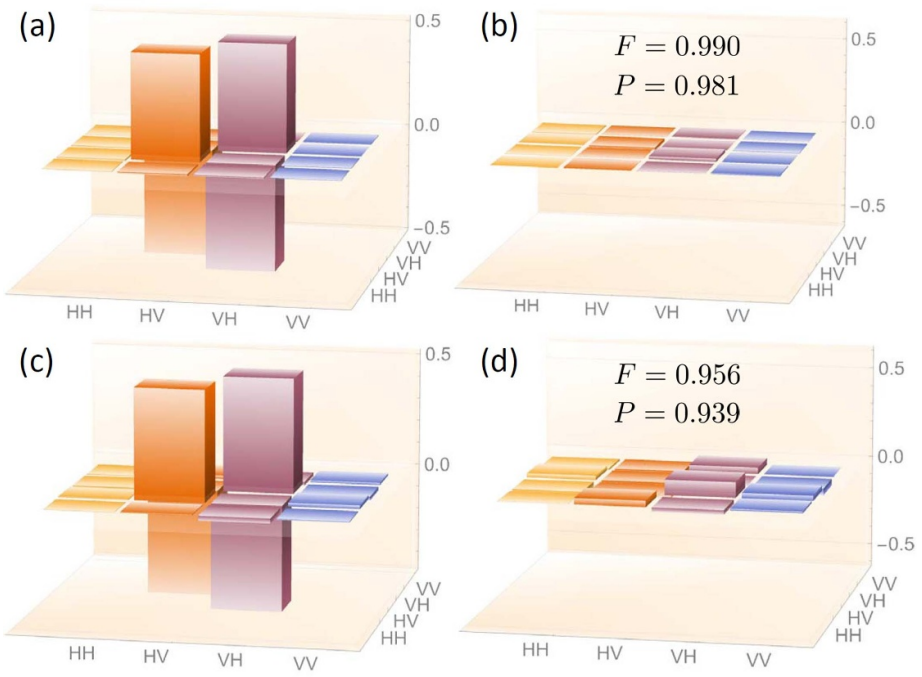

Figure 3. Reconstruction of the two-photon state before and after the Bell parameter measurement. Plots (a) and (b), respectively: real and imaginary part of the quantum tomographic reconstruction of the density matrix of the entangled state undergoing the WMs needed for the single-pair evaluation of the Bell parameter. The good agreement between the reconstructed density matrix and the theoretically expected one $\rho_{\psi_-} = |\psi_-\rangle\langle\psi_-|$ is certified by the quantum Fidelity F reported in the inset of plot (b), together with the reconstructed state Purity P. Plots (c) and (d), respectively: real and imaginary part of the quantum tomographic reconstruction of the density matrix of the entangled state after the WMs. Again, in the inset of plot (d) we report the Fidelity of the state with the singlet state ρ_{ψ_-}, as well as the state Purity. The high value of both parameters provides evidence of the slight disturbance induced on the entangled state by the measurement process (instead of the full wave function collapse), leaving the initial entanglement within the state almost intact.

exploit some optimal estimators [55–57] suited for this family of entangled states, achieving, without having to implement the full quantum state tomography procedure, $\mathcal{N}^{\text{in}} = \mathcal{C}^{\text{in}} = 0.983 \pm 0.001$ and $\mathcal{N}^{\text{out}} = \mathcal{C}^{\text{out}} = 0.927 \pm 0.001$. Aside from the good agreement between the outcomes of these two estimation methods, the extracted Negativity and Concurrence values show how the entanglement of each photon pair is almost entirely preserved during the Bell parameter measurement, leaving it available for other purposes, e.g. for further protocols in quantum information, quantum metrology and related quantum technologies. This is an unprecedented feature in testing Bell inequalities and, more generally, in quantum foundations investigations, since all other experiments so far (even those partially exploiting weak-interaction-based measurements, like in [43–45]) involved final strong measurements collapsing the entangled state and, as a consequence, destroying the entanglement.

3. Conclusion

In conclusion, our result stands out as a unicum in the framework of Bell inequality tests, and even in the one of quantum measurement itself. This will have a substantial impact on foundations of quantum mechanics; indeed, by removing the need to choose among different measurement bases, our approach stretches the concept of counterfactual definiteness, since, by allowing to measure at the same time in all bases, it avoids counterfactual reasoning [14] of the previous Bell inequalities tests.

Although in this experiment we do not close the three main loopholes, in principle they could be closed with a more refined version of our scheme. The detection loophole by exploiting high-efficiency detectors and low-loss optical equipment. The freedom-of-choice loophole by having Alice and Bob still performing two weak measurements in a row, but with two possible sets of settings $\left(\left[\alpha_1^{(a)}, \alpha_2^{(a)}\right]\right.$ and $\left.\left[\beta_1^{(b)}, \beta_2^{(b)}\right]\right)$, respectively, with $a, b = 1, 2$ determined by independent random number generators); by choosing $\left\{\left[\alpha_1^{(1)} = 0, \alpha_2^{(1)} = \frac{\pi}{4}\right];\ \left[\alpha_1^{(2)} = \frac{\pi}{2}, \alpha_2^{(2)} = \frac{3\pi}{4}\right];\ \left[\beta_1^{(1)} = -\frac{3\pi}{8}, \beta_2^{(1)} = \frac{3\pi}{8}\right];\ \left[\beta_1^{(2)} = -\frac{\pi}{8}, \beta_2^{(2)} = \frac{\pi}{8}\right]\right\}$, Alice and Bob obtain the maximal violations $\mathcal{S} = 2\sqrt{2}$ for $a = b$ and $\mathcal{S} = -2\sqrt{2}$ for $a \neq b$. Finally, the locality

loophole can be closed by checking that the entangled pair generation and the measurement choice, as well as photon detection in Alice's and Bob's labs are spacelike-separated events.

Our work does not only pave the way to a new generation of experiments addressed to quantum foundations investigation, but also represents a tool of the utmost interest for quantum technologies, e.g. allowing non-destructive tests of entangled states as a resource and enabling real-time detection of entanglement during quantum computation and simulation schemes or during entanglement-based quantum key distribution protocols. Indeed, after the four WMs in our scheme, the polarization information needed to estimate the Bell parameter is transferred to the spatial domain by the four weak couplings; provided that one pays attention to keep this information intact, one can always realize a second polarization-based protocol in cascade (before the photons arrive to the spatially-resolving detectors), retrieving the information on both protocols once the photon pairs are detected. In particular, our scheme will provide a formidable method for characterizing entanglement in situations where one disposes, as a resource, of several identical entangled pairs; indeed, by keeping an extremely faint interaction with the measuring apparatus, one can obtain a reliable average information on the entangled state realized without sacrificing even a small fraction of the pairs produced, thus maximizing the quantum resources exploitation.

It would be interesting, in a quantum information protocol, to compare the quantum resources (i.e. entangled pairs) spent for characterizing entanglement with traditional (projective) measurements, and the amount of overall information degradation caused by the disturbance induced by our WM-based method on the entangled pairs used, provided that the same precision on the entanglement characterization is achieved. This could allow finding a trade-off between the two methods, and choose between them depending on the amount of resources available and the robustness to noise of the task to be executed; we leave such an analysis for further investigation.

Data availability statement

The data cannot be made publicly available upon publication because they are not available in a format that is sufficiently accessible or reusable by other researchers. The data that support the findings of this study are available upon reasonable request from the authors.

Acknowledgments

This work was financially supported by the projects QuaFuPhy (call 'Trapezio' of Fondazione San Paolo) and AQuTE (MUR, call 'PRIN 2022', grant No. 2022RATBS4), by the Israel Innovation Authority under Grants 70002 and 73795, by the Elta Systems Ltd the Pazy Foundation, the Israeli Ministry of Science and Technology, and by the Quantum Science and Technology Program of the Israeli Council of Higher Education. This work was also funded by the Project EMPIR 19NRM06 METISQ. This project received funding by the EMPIR program cofinanced by the Participating States and from the European Union Horizon 2020 Research and Innovation Programme. The results presented in this article had been achieved also in the context of the following projects: QUID (QUantum Italy Deployment) and EQUO (European QUantum ecOsystems), which are funded by the European Commission in the Digital Europe Programme under the Grant Agreement Numbers 101091408 and 101091561; QU-TEST, which had received funding from the European Union's Horizon Europe under the Grant Agreement Number 101113901. We thank Yakir Aharonov and Avshalom Elitzur for enlightening discussions, and Federico Maestri and Matteo Bevilacqua for contributing to the initial phase of the experimental setup implementation.

Appendix A. Experimental details

A detailed scheme of the experimental setup is presented in figure A1. A CW pump laser at 405 nm enters a Sagnac interferometer, hosting a periodically-poled Potassium Titanyl-Phosphate (PPKTP) crystal in which degenerate collinear Type-II Spontaneous Parametric Down-Conversion (SPDC) occurs, creating orthogonally-polarized photon pairs at 810 nm. The L_P1 and L_P2 lenses are placed to obtain a Gaussian beam with the waist close to the center of the PPKTP crystal. An optical isolator (OI) avoids possible back-reflections to the laser source and selects the laser light to be in a linear polarization, whose axis is eventually rotated by a half-wave plate (HWP_P). A dichroic mirror (DM_B) sends the pump both to the clockwise and counterclockwise paths of the Sagnac interferometer, allowing to create polarization-entangled photon pairs. Specifically, the DM_B, highly reflective for the pump and highly transmissive for the down-converted photons, addresses the pump laser to the polarizing beam splitter (PBS). Here, the beam is

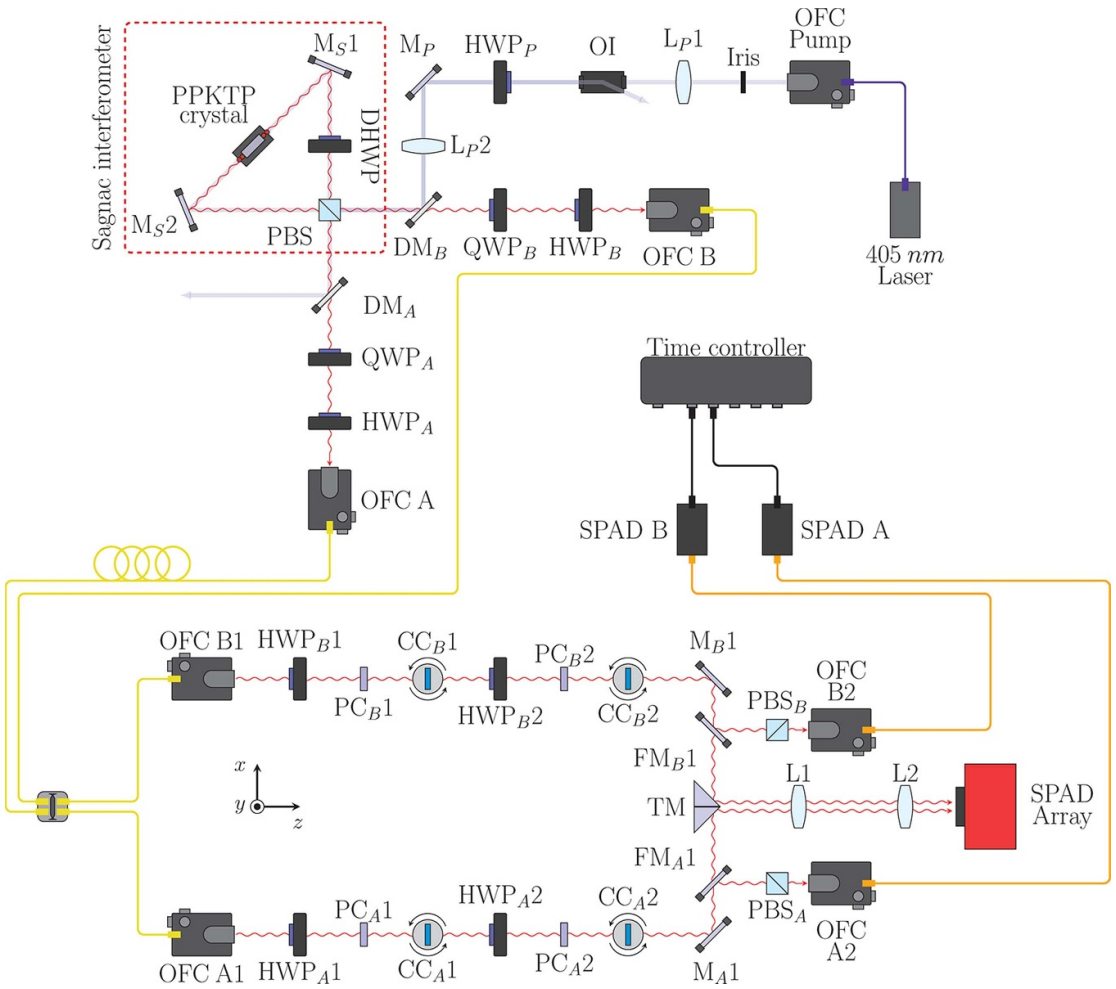

Figure A1. Detailed scheme of the experimental setup. Polarization-entangled photons are generated in a Sagnac interferometer, fiber coupled and then collimated in a Gaussian spatial mode. Then, each of them undergoes two weak measurements in sequence, each realized by a pair of birefringent crystals preceded by a half-wave plate, before impinging on a 24 × 24 SPAD array detecting the photon pairs with 2D spatial resolution. OFC: Optical fiber coupler; L: lens; OI: Optical isolator; HWP: Half-wave plate; QWP: Quarter-wave plate; DHWP: Dual half-wave plate; DM: Dichroic mirror; M: Mirror; PBS: Polarizing beam splitter; PC: Principal crystal; CC: Compensation crystal; TM: Triangular mirror; PPKTP: periodically-poled Potassium Titanyl-Phosphate; SPAD: Single photon avalanche diode.

split between the H (clockwise path) and V (counterclockwise path) polarizations, and sent to the PPKTP crystal by two high-reflecting mirrors (M_s1 and M_s2). A dual wavelength half-wave plate (DHWP), with an angle of 45° with respect to the horizontal plane is inserted between the PBS and the PPKTP crystal in the counterclockwise path, so that in both paths the pump enters the PPKTP crystal horizontally-polarized, generating Type-II SPDC. The two photons of each down-converted pair produced in both paths are separated by the PBS and sent, respectively, to the A and B branches, with a finely-tuned relative phase set in order to form the singlet state $|\psi_-\rangle = (|H_A V_B\rangle - |V_A H_B\rangle)/\sqrt{2}$, being $H(V)$ the horizontal (vertical) polarization component. Dichroic mirrors ($\mathrm{DM}_{A(B)}$) stop the pump transmission, whereas they allow the down-converted photons to pass through. The down-converted photons are then spectrally filtered, coupled to single-mode fibers and then collimated into Gaussian spatial modes $|f_{x_{A(B)}}\rangle \otimes |f_{y_{A(B)}}\rangle$ (with $\langle \xi | f_\xi \rangle = \frac{1}{(2\pi\sigma^2)^{1/4}} \exp\left(-\frac{\xi^2}{4\sigma^2}\right)$, being $\xi = x, y$ and σ the Gaussian width in both the x and y directions), addressed to two symmetrical branches (A, B) in which the weak measurements in sequence take place. Specifically, the preliminary calibration of our setup yielded, for the initial Gaussian distributions in the two branches, $\sigma_A = 1.722 \pm 0.017$ and $\sigma_B = 1.863 \pm 0.015$ (in pixel units).

The combination of quarter- and half-wave plates ($\mathrm{QWP}_{A(B)}$ and $\mathrm{HWP}_{A(B)}$, respectively) is used to compensate the polarization changes due to the single-mode fibers. This way, we are able to initialize the $|\psi_-\rangle$ state with visibility $V^{\mathrm{in}} = 0.983 \pm 0.001$, being $V = \frac{N(+,-)+N(-,+)-N(+,+)-N(-,-)}{N(+,-)+N(-,+)+N(+,+)+N(-,-)}$, $N(\circ,\diamond)$ the two-photon counts registered while projecting photons A and B onto the $|\circ\rangle$ and $|\diamond\rangle$ states (respectively) and

$|\pm\rangle = \frac{1}{\sqrt{2}}(|H\rangle \pm |V\rangle)$. Such a high visibility clearly highlights the good quality of the entangled state produced by our Sagnac interferometer.

The initial bipartite state, then, takes the form $|\Psi_{\rm in}\rangle = |\psi_-\rangle \otimes |f_{x_A}\rangle \otimes |f_{y_A}\rangle \otimes |f_{x_B}\rangle \otimes |f_{y_B}\rangle$.

In both branches A and B, the sequence of WMs needed for evaluating the Bell parameter is implemented by exploiting the weak coupling between polarization and transverse momentum induced by two thin calcite ($CaCO_3$) crystal pairs. In each pair, the principal crystal ($PC_{A(B)}$) induces a tiny spatial walk-off (on a transverse direction with respect to the photon propagation) between the H and V polarization components, together with the temporal separation and phase delay. The compensation crystal $CC_{A(B)}$, instead, is used to recover the temporal delay and restore the proper phase without introducing any further spatial decoherence. The optical e-axes of $PC_{A(B)}1$ and $PC_{A(B)}2$ lie, respectively, along perpendicular planes, i.e. $z-x$ and $y-z$, in order to induce the spatial walk-off in the two independent transverse directions, namely x and y. A pair of half-wave plates in each branch ($HWP_{A(B)}1$ and $HWP_{A(B)}2$) allows performing WMs of different (non-commuting) polarizations. Essentially, the ensemble of HWPs and crystal pairs is set in order to realize the entangling unitary transformation:

$$\hat{U}_{\xi_{jK}} = \exp\left(-\frac{i}{\hbar} g_{\xi_{jK}} \hat{\Pi}\left(\theta_{Kj}\right) \otimes \hat{P}_{\xi_{jK}}\right), \tag{A1}$$

where $g_{\xi_{jK}} \ll 1$ is the weak coupling constant connected with the spatial degree of freedom ξ_{jK} ($K = A, B$, $j = 1, 2$, $\xi_1 = x$, $\xi_2 = y$), $\hat{\Pi}(\theta_{Kj})$ represents the polarization projector along a direction described by the angle θ_{K_j} ($\theta_A = \alpha$, $\theta_B = \beta$) , and $\hat{P}_{\xi_{jK}}$ is the transverse momentum of the photon on the optical plane of the crystal (for a detailed analysis of the WM dependence on the actual value of $g_{\xi_{jK}}$, see e.g. [58]). Then, the photons are sent to a 24×24 Single Photon Avalanche Diode (SPAD) array, i.e. a single photon detector with 2D spatial resolution recording the arrival time and position of each detected photon [59]. The L1 and L2 lenses constitute an imaging system needed to match the photon spatial distributions dimensions with the ones of the SPAD array active area.

Thanks to the internal time-tagger of the SPAD array, it is possible to extract the coincidence counts tensor $N(X_A, Y_A, X_B, Y_B)$, being X_A, Y_A and X_B, Y_B the coordinates in which the two photon constituting the entangled pair impinge.

Specifically, $N(X_A, Y_A, X_B, Y_B)$ is evaluated by considering that our SPAD array registers, pixelwise, the time stamps (with respect to an internal clock) of the photon detections occurred. Coincidences are evaluated by using a 'click' in channel A detector region as a trigger, and registering the time stamps of the subsequent detection events in channel B detector region. Coincidence counts are defined as two-count events (between A and B) occurring within a temporal window of ~ 2 ns (chosen while taking into account the detector jitter) centered on the delay due to the optical path difference between the two channels. Then, accidental coincidences are evaluated by estimating the average number of events per time bin outside of the coincidence window, and subtracted from each time bin belonging to the coincidence window.

The $N(X_A, Y_A, X_B, Y_B)$ tensor can be used to evaluate, for each detected pair, the entire Bell parameter $\mathcal{S}$. Indeed, one can demonstrate that, considering only projections onto the real plane of the Bloch sphere, after the entangled state undergoes the four weak interactions one has

$$\langle \hat{\xi}_{jA} \otimes \hat{\xi}_{lB} \rangle_{\rm out} = \langle \Psi_{\rm out} | \hat{\xi}_{jA} \otimes \hat{\xi}_{lB} | \Psi_{\rm out} \rangle \simeq g_{\xi_{jA}} g_{\xi_{lB}} \langle \psi_- | \hat{\Pi}\left(\alpha_j\right) \otimes \hat{\Pi}\left(\beta_l\right) | \psi_- \rangle \tag{A2}$$

and

$$\langle \hat{\xi}_{jK} \rangle_{\rm out} = \langle \Psi_{\rm out} | \hat{\xi}_{jK} | \Psi_{\rm out} \rangle \simeq g_{\xi_{jK}} \langle \psi_- | \hat{\Pi}\left(\theta_{Kj}\right) | \psi_- \rangle, \tag{A3}$$

where $j, l = 1, 2$, $\hat{\xi}_1 = X$, $\hat{\xi}_2 = Y$, $\hat{\Pi}(\theta_{Kj}) = \frac{I + \sigma_z(\theta_{Kj})}{2}$ and $|\Psi_{\rm out}\rangle = U_{x_A} U_{x_B} U_{y_A} U_{y_B} |\Psi_{\rm in}\rangle$ is the bipartite state outgoing the measurement process. Then, the correlation $C(\alpha_j, \beta_l)$ can be written as:

$$C\left(\alpha_j, \beta_l\right) = \langle \hat{\sigma}_z\left(\alpha_j\right) \otimes \hat{\sigma}_z\left(\beta_l\right) \rangle = 4 \frac{\langle \hat{\xi}_{jA} \otimes \hat{\xi}_{lB} \rangle}{g_{\xi_{jA}} g_{\xi_{lB}}} - 2 \frac{\langle \hat{\xi}_{jA} \rangle}{g_{\xi_{jA}}} - 2 \frac{\langle \hat{\xi}_{lB} \rangle}{g_{\xi_{lB}}} + 1, \tag{A4}$$

and, from that, the Bell parameter $\mathcal{S}$ can be evaluated as:

$$\mathcal{S}^{\rm ave} = \langle \mathcal{S} \rangle_{\rm out} = 4 \left\langle \frac{\hat{X}_A \otimes \hat{X}_B}{g_{x_A} g_{x_B}} + \frac{\hat{Y}_A \otimes \hat{X}_B}{g_{y_A} g_{x_B}} - \frac{\hat{X}_A \otimes \hat{Y}_B}{g_{x_A} g_{y_B}} + \frac{\hat{Y}_A \otimes \hat{Y}_B}{g_{y_A} g_{y_B}} - \frac{\hat{Y}_A}{g_{y_A}} - \frac{\hat{X}_B}{g_{x_B}} \right\rangle_{\rm out} + 2. \tag{A5}$$

Eventually, the flipping mirrors FM_A1 and FM_B1 allow sending the photons to a projective measurement apparatus, comprising, in each branch, a QWP+HWP+PBS set (not shown in the figure) followed by a SPAD working as a bucket detector. The outputs of SPAD A and B are then addressed to a time-tagging controller. With this alternative configuration, we can fully characterize the state by performing a quantum tomographic reconstruction [52] of its density matrix.

Appendix B. Measurement procedure and statistical analysis

In our experiment, we perform five data acquisitions, with different setup configurations. The first two acquisitions, required for calibrating the system, consist in sending only H or V photons in each of the two A and B branches of the experimental setup (figure A1). To do this, we set, in both measurement branches, the half-wave plates rotation angles to 0, and the pump half-wave plate HWP_P in order to enter the Sagnac interferometer either clockwise or counterclockwise, generating, respectively, the two-photon separable states $|H_A V_B\rangle$ and $|V_A H_B\rangle$. This way, since the first(second) birefringent crystal pair in each branch shifts the horizontally(vertically)-polarized photons along the $x(y)$ axis, we obtain the centers of the distributions corresponding to the two polarizations paths via a linear regression of several subsets and a subsequent average. We dub the center of the unperturbed (shifted) spatial distribution of the photon as $\tilde{\xi}_{iK,0(1)}$ $(i=1,2;$ $K=A,B)$.

Subsequently, we acquire a data set for the Bell parameter estimation, from which we obtain a set of ξ_{iK} values for the four coordinates. Finally, we remove the birefringent crystals and perform two data acquisitions with only the half-wave plates set, respectively, at the rotation angles for the Bell parameter estimation and at the 0 rotation position. We do this to evaluate, by linear regression and subsequent average, the unwanted spatial deviation induced on the photons by the different half-wave plate angles between calibration and CHSH acquisition, which we dub as $\tilde{\xi}_{iK,\mathrm{shift}}$.

As stated in appendix A, simple algebra shows that the explicit expression for the Bell parameter $\mathcal{S}$ reads:

$$\mathcal{S}^{\mathrm{ave}} = 4\left\langle \frac{\hat{\xi}_{1A}\otimes\hat{\xi}_{1B}}{g_{1A}g_{1B}} + \frac{\hat{\xi}_{2A}\otimes\hat{\xi}_{1B}}{g_{2A}g_{1B}} - \frac{\hat{\xi}_{1A}\otimes\hat{\xi}_{2B}}{g_{1A}g_{2B}} + \frac{\hat{\xi}_{2A}\otimes\hat{\xi}_{2B}}{g_{2A}g_{2B}} - \frac{\hat{\xi}_{2A}}{g_{2A}} - \frac{\hat{\xi}_{1B}}{g_{1B}} \right\rangle_{\mathrm{out}} + 2\,. \tag{B1}$$

The terms $\langle\hat{\xi}_{iK}\rangle_{\mathrm{out}}$ $(i=1,2;K=A,B)$ and $\langle\hat{\xi}_{iA}\otimes\hat{\xi}_{jB}\rangle_{\mathrm{out}}$ $(i,j=1,2)$ can be evaluated as

$$\langle\hat{\xi}_{iK}\rangle_{\mathrm{out}} = \left\langle \xi_{iK} - \tilde{\xi}_{iK,0} - \tilde{\xi}_{iK,\mathrm{shift}} \right\rangle_{\mathrm{out}} \tag{B2}$$

$$\left\langle\hat{\xi}_{iA}\otimes\hat{\xi}_{jB}\right\rangle_{\mathrm{out}} = \left\langle \left(\xi_{iA} - \tilde{\xi}_{iA,0} - \tilde{\xi}_{iA,\mathrm{shift}}\right)\left(\xi_{jB} - \tilde{\xi}_{jB,0} - \tilde{\xi}_{jB,\mathrm{shift}}\right)\right\rangle_{\mathrm{out}}, \tag{B3}$$

being $g_{iK} = \tilde{\xi}_{iK,1} - \tilde{\xi}_{iK,0}$ $(i=1,2;K=A,B)$ the interaction strength of each measurement.

By expanding the average, the Bell parameter can be written as:

$$\begin{aligned}
\mathcal{S}^{\mathrm{ave}} = 4\Bigg\langle & \frac{\left(\xi_{1A} - \tilde{\xi}_{1A,0} - \tilde{\xi}_{1A,\mathrm{shift}}\right)\left(\xi_{1B} - \tilde{\xi}_{1B,0} - \tilde{\xi}_{1B,\mathrm{shift}}\right)}{\left(\tilde{\xi}_{1A,1} - \tilde{\xi}_{1B,0}\right)\left(\tilde{\xi}_{1B,1} - \tilde{\xi}_{1B,0}\right)} \\
& + \frac{\left(\xi_{2A} - \tilde{\xi}_{2A,0} - \tilde{\xi}_{2A,\mathrm{shift}}\right)\left(\xi_{1B} - \tilde{\xi}_{1B,0} - \tilde{\xi}_{1B,\mathrm{shift}}\right)}{\left(\tilde{\xi}_{2A,1} - \xi_{2A,0}\right)\left(\tilde{\xi}_{1B,1} - \tilde{\xi}_{1B,0}\right)} \\
& - \frac{\left(\xi_{1A} - \tilde{\xi}_{1A,0} - \tilde{\xi}_{1A,\mathrm{shift}}\right)\left(\xi_{2B} - \tilde{\xi}_{2B,0} - \tilde{\xi}_{2B,\mathrm{shift}}\right)}{\left(\tilde{\xi}_{1A,1} - \xi_{1A,0}\right)\left(\tilde{\xi}_{2B,1} - \tilde{\xi}_{2B,0}\right)} \\
& + \frac{\left(\xi_{2A} - \tilde{\xi}_{2A,0} - \tilde{\xi}_{2A,\mathrm{shift}}\right)\left(\xi_{2B} - \tilde{\xi}_{2B,0} - \tilde{\xi}_{2B,\mathrm{shift}}\right)}{\left(\tilde{\xi}_{2A,1} - \xi_{2A,0}\right)\left(\tilde{\xi}_{2B,1} - \tilde{\xi}_{2B,0}\right)} \\
& - \frac{\xi_{2A} - \tilde{\xi}_{2A,0} - \tilde{\xi}_{2A,\mathrm{shift}}}{\tilde{\xi}_{2A,1} - \tilde{\xi}_{2A,0}} - \frac{\xi_{1B} - \tilde{\xi}_{1B,0} - \tilde{\xi}_{1B,\mathrm{shift}}}{\tilde{\xi}_{1B,1} - \tilde{\xi}_{1B,0}} \Bigg\rangle_{\mathrm{out}} + 2
\end{aligned} \tag{B4}$$

Table B1. Uncertainty budget for the average value of the Bell parameter $\mathcal{S}$ estimated in our experiment. $\sigma_{\mathcal{S}}$: total uncertainty. σ_{stat}: statistical uncertainty contribution. σ_{cal}: uncertainty contribution due to the setup calibration procedure. σ_{shift}: uncertainty contribution connected with the correction of the unwanted spatial shifts caused by the half-wave plates.

$\mathcal{S}^{\text{ave}}$	$\sigma_{\mathcal{S}^{\text{ave}}}$	σ_{stat}	σ_{cal}	σ_{shift}
-2.79	0.14	0.09	0.11	0.02

or, equivalently:

$$\begin{aligned}\mathcal{S}^{\text{ave}} = \frac{4}{N}\sum_{n=1}^{N}\Bigg(&\frac{\left(\xi_{1A}^{(n)}-\tilde{\xi}_{1A,0}-\tilde{\xi}_{1A,\text{shift}}\right)\left(\xi_{1B}^{(n)}-\tilde{\xi}_{1B,0}-\tilde{\xi}_{1B,\text{shift}}\right)}{\left(\tilde{\xi}_{1A,1}-\tilde{\xi}_{1B,0}\right)\left(\tilde{\xi}_{1B,1}-\tilde{\xi}_{1B,0}\right)}\\ &+\frac{\left(\xi_{2A}^{(n)}-\tilde{\xi}_{2A,0}-\tilde{\xi}_{2A,\text{shift}}\right)\left(\xi_{1B}^{(n)}-\tilde{\xi}_{1B,0}-\tilde{\xi}_{1B,\text{shift}}\right)}{\left(\tilde{\xi}_{2A,1}-\xi_{2A,0}\right)\left(\tilde{\xi}_{1B,1}-\tilde{\xi}_{1B,0}\right)}\\ &-\frac{\left(\xi_{1A}^{(n)}-\tilde{\xi}_{1A,0}-\tilde{\xi}_{1A,\text{shift}}\right)\left(\xi_{2B}^{(n)}-\tilde{\xi}_{2B,0}-\tilde{\xi}_{2B,\text{shift}}\right)}{\left(\tilde{\xi}_{1A,1}-\xi_{1A,0}\right)\left(\tilde{\xi}_{2B,1}-\tilde{\xi}_{2B,0}\right)}\\ &+\frac{\left(\xi_{2A}^{(n)}-\tilde{\xi}_{2A,0}-\tilde{\xi}_{2A,\text{shift}}\right)\left(\xi_{2B}^{(n)}-\tilde{\xi}_{2B,0}-\tilde{\xi}_{2B,\text{shift}}\right)}{\left(\tilde{\xi}_{2A,1}-\xi_{2A,0}\right)\left(\tilde{\xi}_{2B,1}-\tilde{\xi}_{2B,0}\right)}\\ &-\frac{\xi_{2A}^{(n)}-\tilde{\xi}_{2A,0}-\tilde{\xi}_{2A,\text{shift}}}{\tilde{\xi}_{2A,1}-\tilde{\xi}_{2A,0}}-\frac{\xi_{1B}^{(n)}-\tilde{\xi}_{1B,0}-\tilde{\xi}_{1B,\text{shift}}}{\tilde{\xi}_{1B,1}-\tilde{\xi}_{1B,0}}\Bigg)+2\,,\end{aligned} \tag{B5}$$

where n indicates the nth detection event ($n=1,\ldots,N$) and $\xi_{iK}^{(n)}$ are the corresponding detection coordinates ($i=1,2;K=A,B$).

The experimental uncertainty associated with $\mathcal{S}^{\text{ave}}$ is evaluated as:

$$\sigma_{\mathcal{S}^{\text{ave}}} = \left(\sigma_{\text{stat}}^2+\sum_{\substack{i=1,2\\K=A,B\\j=0,1}}\left(\frac{\partial\mathcal{S}}{\partial\tilde{\xi}_{iK,j}}\right)^2\sigma_{\tilde{\xi}_{iK,j}}^2+\sum_{\substack{i=1,2\\K=A,B}}\left(\frac{\partial\mathcal{S}}{\partial\tilde{\xi}_{iK,\text{shift}}}\right)^2\sigma_{\tilde{\xi}_{iK,\text{shift}}}^2\right)^{1/2}, \tag{B6}$$

where σ_{stat} is the statistical uncertainty contribution, evaluated as the uncertainty on the average, $\sigma_{\tilde{\xi}_{iX,j}}$ ($i=1,2;X=A,B;j=0,1$) is the uncertainty associated with the calibration procedure, $\sigma_{\tilde{\xi}_{iX,\text{shift}}}$ is the uncertainty due to the spatial shift induced by the half-wave plates. Given the very small amount of accidental coincidence events, the uncertainty contribution associated with them turns out to be negligible and can be omitted.

The uncertainty budget is reported in table B1. The quantities:

$$\sigma_{\text{cal}} = \sqrt{\sum_{\substack{i=1,2\\K=A,B\\j=0,1}}\left(\frac{\partial\mathcal{S}}{\partial\tilde{\xi}_{iK,j}}\right)^2\sigma_{\tilde{\xi}_{iK,j}}^2} \tag{B7}$$

$$\sigma_{\text{shift}} = \sqrt{\sum_{\substack{i=1,2\\K=A,B}}\left(\frac{\partial\mathcal{S}}{\partial\tilde{\xi}_{iK,\text{shift}}}\right)^2\sigma_{\tilde{\xi}_{iK,\text{shift}}}^2} \tag{B8}$$

correspond to the total uncertainty contributions due to, respectively, the calibration process (σ_{cal}) and the procedure for the correction of the spatial deviations caused by the wave plates (σ_{shift}):

ORCID iDs

Salvatore Virzì https://orcid.org/0000-0002-9067-5970
Enrico Rebufello https://orcid.org/0000-0002-8374-1976
Francesco Atzori https://orcid.org/0009-0008-0499-9014
Alessio Avella https://orcid.org/0000-0002-2148-6228
Fabrizio Piacentini https://orcid.org/0000-0002-8098-5692
Marco Gramegna https://orcid.org/0000-0002-5725-0444
Eliahu Cohen https://orcid.org/0000-0001-6198-0725
Ivo Pietro Degiovanni https://orcid.org/0000-0003-0332-3115
Marco Genovese https://orcid.org/0000-0001-9186-8849

References

[1] Bell J S 1965 On the Einstein Podolsky Rosen paradox *Physics* **1** 195
[2] Genovese M 2005 Research on hidden variable theories: a review of recent progresses *Phys. Rep.* **413** 319–96
[3] Brunner N, Cavalcanti D, Pironio S, Scarani V and Wehner S 2013 Bell nonlocality *Rev. Mod. Phys.* **86** 419
[4] Myrvold W, Genovese M and Shimony A 2021 Bell's Theorem *The Stanford Encyclopedia of Philosophy* ed E N Zalta (Metaphysics Research Lab, Stanford University)
[5] Georgescu I 2021 How the bell tests changed quantum physics *Nat. Rev. Phys.* **3** 674
[6] Ekert A K 1991 Quantum cryptography based on Bell's theorem *Phys. Rev. Lett.* **67** 661
[7] Hensen B *et al* 2015 Loophole-free Bell inequality violation using electron spins separated by 1.3 km *Nature* **526** 682
[8] Giustina M *et al* 2015 Significant-loophole-free test of Bell's Theorem with entangled photons *Phys. Rev. Lett.* **115** 250401
[9] Shalm L K 2015 Strong loophole-free test of local realism *Phys. Rev. Lett.* **115** 250402
[10] Aharonov Y, Albert D Z and Vaidman L 1988 How the result of a measurement of a component of the spin of a spin-1/2 particle can turn out to be 100 *Phys. Rev. Lett.* **60** 1351
[11] Kofman A G, Ashhab S and Nori F 2012 Nonperturbative theory of weak pre-and post-selected measurements *Phys. Rep.* **520** 43
[12] Tamir B and Cohen E 2013 Introduction to weak measurements and weak values *Quanta* **3** 7
[13] Dressel J, Malik M, Miatto F M, Jordan A N and Boyd R W 2014 Colloquium: understanding quantum weak values: basics and applications *Rev. Mod. Phys.* **86** 307
[14] Aharonov Y, Botero A, Popescu S, Reznik B and Tollaksen J 2002 Revisiting hardy's paradox: counterfactual statements, real measurements, entanglement and weak values *Phys. Lett.* A **301** 130
[15] Genovese M and Gramegna M 2019 Quantum correlations and quantum non-locality: a review and a few new ideas *Appl. Sci.* **9** 5406
[16] Freedman J S and Clauser J F 1972 Experimental test of local hidden-variable theories *Phys. Rev. Lett.* **28** 938
[17] Kasday L R, Ullman J D and Wu C S 1975 Angular correlation of Compton-scattered annihilation photons and hidden variables *Nuovo Cimento* B **25** 633
[18] Clauser J F 1976 Experimental investigation of a polarization correlation anomaly *Phys. Rev. Lett.* **36** 1223
[19] Aspect A, Dalibard J and Roger G 1982 Experimental test of Bell's inequalities using time-varying analyzers *Phys. Rev. Lett.* **49** 1804
[20] Masa E Ares L and Luis A 2020 Nonclassical joint distributions and bell measurements *Phys. Lett.* A **384** 126416
[21] Silva R, Gisin N, Guryanova Y and Popescu S 2015 Multiple observers can share the nonlocality of half of an entangled pair by using optimal weak measurements *Phys. Rev. Lett.* **114** 250401
[22] Ritchie N W M, Story J G and Hulet R G 1991 Realization of a measurement of a weak value *Phys. Rev. Lett.* **66** 1107
[23] Mitchison G, Jozsa R and Popescu S 2007 Sequential weak measurement *Phys. Rev.* A **76** 062105
[24] Aharonov Y, Cohen E and Elitzur A 2015 Can a future choice affect a past measurement's outcome? *Ann. Phys.* **355** 258–68
[25] Thekkadath G S, Giner L, Chalich Y, Horton M J, Banker J and Lundeen J S 2016 Direct measurement of the density matrix of a quantum system *Phys. Rev. Lett.* **117** 120401
[26] Piacentini F *et al* 2016 Measuring incompatible observables by exploiting sequential weak values *Phys. Rev. Lett.* **117** 120402
[27] Kim Y, Kim Y S, Lee S Y, Moon S, Kim Y H and Cho Y W 2018 direct quantum process tomography via measuring sequential weak values of incompatible observables *Nat. Commun.* **9** 192
[28] Foletto G, Padovan M, Avesani M, Tebyanian H, Villoresi P and Vallone G 2021 Experimental test of sequential weak measurements for certified quantum randomness extraction *Phys. Rev.* A **103** 062206
[29] Hosten O and Kwiat P 2008 Observation of the spin hall effect of light via weak measurements *Science* **319** 787
[30] Kim Y S, Lee J C, Kwon O and Kim Y H 2012 Protecting entanglement from decoherence using weak measurement and quantum measurement reversal *Nat. Phys.* **8** 117
[31] Hallaji M, Feizpour A, Dmochowski G, Sinclair J and Steinberg A M 2017 Weak-value amplification of the nonlinear effect of a single photon *Nat. Phys.* **13** 540
[32] Piacentini F *et al* 2016 Experiment investigating the connection between weak values and contextuality *Phys. Rev. Lett.* **116** 180401
[33] Waegell M, Denkmayr T, Geppert H, Ebner D, Jenke T, Hasegawa Y, Sponar S, Dressel J and Tollaksen J 2017 Confined contextuality in neutron interferometry: observing the quantum pigeonhole effect *Phys. Rev.* A **96** 052131
[34] Cimini V, Gianani I, Piacentini F, Degiovanni I P and Barbieri M 2020 Anomalous values, fisher information and contextuality, in generalized quantum measurements *Quantum Sci. Technol.* **5** 025007
[35] Mahler D H, Rozema L, Fisher K, Vermeyden L, Resch K J, Wiseman H M and Steinberg A 2016 Experimental nonlocal and surreal Bohmian trajectories *Sci. Adv.* **2** e150146
[36] Hu M J, Zhou Z Y, Hu X M, Li C F, Guo G C and Zhang Y S 2018 Observation of non-locality sharing among three observers with one entangled pair via optimal weak measurement *npj Quantum Inf.* **4** 63
[37] Jordan A N, Korotkov A N and Büttiker M 2006 Leggett-Garg inequality with a kicked quantum pump *Phys. Rev. Lett.* **97** 026805
[38] Williams N S and Jordan A N 2008 Weak values and the Leggett-Garg inequality in solid-state qubits *Phys. Rev. Lett.* **100** 026804
[39] Groen J P, Ristè D, Tornberg L, Cramer J, de Groot P C, Picot T, Johansson G and DiCarlo L 2013 Partial-measurement backaction and nonclassical weak values in a superconducting circuit *Phys. Rev. Lett.* **111** 090506

[40] Goggin M E, Almeida P M, Barbieri M, Lanyon B P, O'Brien J L, White A G and Pryde G J 2011 Violation of the Leggett-Garg inequality with weak measurements of photons *PNAS* **108** 1256
[41] Avella A *et al* 2017 Anomalous weak values and the violation of a multiple-measurement Leggett-Garg inequality *Phys. Rev.* A **96** 052123
[42] Palacios-Laloy A, Mallet F, Nguyen F, Bertet P, Vion D, Esteve D and Korotkov A N 2010 Experimental violation of a Bell's inequality in time with weak measurement *Nat. Phys.* **6** 442–7
[43] Foletto G *et al* 2020 Experimental certification of sustained entanglement and nonlocality after sequential measurements *Phys. Rev. Appl.* **13** 044008
[44] Calderón-Losada O, Moctezuma Quistian T T, Cruz-Ramirez H, Ramirez S M, U'Ren A B, Botero A and Valencia A 2020 A weak values approach for testing simultaneous Einstein-Podolsky-Rosen elements of reality for non-commuting observables *Commun. Phys.* **3** 117
[45] White T C *et al* 2016 Preserving entanglement during weak measurement demonstrated with a violation of the Bell–Leggett–Garg inequality *npj Quantum Inf.* **2** 15022
[46] Matsuyama K, Hofmann H F and Iinuma M 2021 Experimental investigation of the relation between measurement uncertainties and non-local quantum correlations *J. Phys. Commun.* **5** 115012
[47] Lambare J P 2021 Bell inequalities, counterfactual definiteness and falsifiability *Int. J. Quant. Inf.* **19** 2150018 and references therein
[48] Dieks D 1994 Modal interpretation of quantum mechanics, measurements and macroscopic behavior *Phys. Rev.* A **49** 2290
[49] Auffèves A and Grangier P 2016 Contexts, systems and modalities: a new ontology for quantum mechanics *Found. Phys.* **46** 121
[50] Lundeen J and Steinberg A M 2009 Experimental joint weak measurement on a photon pair as a probe of hardy's paradox *Phys. Rev. Lett.* **102** 020404
[51] Rebufello E *et al* 2021 Anomalous weak values via a single photon detection *Light Sci. Appl.* **10** 106
[52] Bogdanov Y I, Brida G, Genovese M, Kulik S P, Moreva E V and Shurupov A P 2010 Statistical estimation of the efficiency of quantum state tomography protocols *Phys. Rev. Lett.* **105** 010404
[53] Gilchrist A, Langford N K and Nielsen M A 2005 Distance measures to compare real and ideal quantum processes *Phys. Rev.* A **71** 062310
[54] Verstraete F, Audenaert K, Dehaene J and De Moor B 2001 A comparison of the entanglement measures negativity and concurrence *J. Phys. A: Math. Gen.* **34** 10327
[55] Brida G *et al* 2010 Experimental estimation of entanglement at the quantum limit *Phys. Rev. Lett.* **104** 100501
[56] Brida G *et al* 2011 Optimal estimation of entanglement in optical qubit systems *Phys. Rev.* A **83** 052301
[57] Virzì S, Rebufello E, Avella A, Piacentini F, Gramegna M, Ruo Berchera I, Degiovanni I P and Genovese M 2019 Optimal estimation of entanglement and discord in two-qubit states *Sci. Rep.* **9** 3030
[58] Piacentini F, Avella A, Gramegna M, Lussana R, Villa F, Tosi A, Brida G, Degiovanni I P and Genovese M 2018 Investigating the effects of the interaction intensity in a weak measurement *Sci. Rep.* **8** 6959
[59] Madonini F, Severini F, Incoronato A, Conca E and Villa F 2021 Design of a 24x24 SPAD imager for multi-photon coincidence-detection in super resolution microscopy *Proc. SPIE* **11771** 117710B